Rotation Invariant Automatic Infrared Target Recognition using G-Radon

Jin-Ju Won, Sungho Kim

Department of Electronic Engineering Yeungnam University, Gyeonsan, Gyeongbuk, 38541, Korea

Abstract. In recent research, automatic target recognition (ATR) of infrared targets has been taking a lot of interest to the researchers. A rotation invariant method is useful in target recognition, classification and image analysis to reduce the number of training data. In particular, rotation invariant method, Radon transform, is an effective technique that is used for medical care such as computerized tomography (CT) image. This paper proposes a new rotation invariant algorithm for target recognition. The proposed method combines the gradient information and radon transform. The propose method, called gradient Radon (G-Radon), is applied to synthesized infrared images and compared with traditional radon transform and Zernike moments for validation.

1 Introduction

In recent research, ATR of infrared targets has been taking a lot of interest to the researchers [1]. Conventional ATR algorithms [2] are based on the model-based method [3, 4] and learning-based method [5, 6]. Example of model-based research is image classification using hidden markov trees [3]. Learning-based researches are wavelet based target recognition and target recognition using support vector machines (SVM) [5, 6]. Histogram of oriented gradients (HOG) [7] is a famous algorithm with excellent performance when combined with SVM. But these algorithms are sensitive to rotation. Therefore rotation invariant method is necessary in target recognition and classification. The rotation invariant method is useful to reduce the number of training images. The simplest form of rotation invariant feature is the Fourier transformation of the boundary curve which is invariant with regard to translation and rotation [8]. A popular invariant feature is based on the moment including non-orthogonal moments [9]-[11] and orthogonal moments [12]-[14]. These methods have property such as less sensitive to noise and very accurate in image reconstruction. Scale invariant feature transform (SIFT) also has the property that for size invariant and rotation invariant. SIFT selects the local maxima and generates a descriptor as feature points by using a histogram of the surrounding area in an image. This method serves to strength the distortion or partial change of the image, but a significant amount of calculation occurs to generate the feature vector of 128 dimensions [15, 16].

This paper uses image gradient to extract target contour and Radon transform to extract rotation invariant feature. Radon transform is an effective technique that is used for medical care such as CT images. We propose a

gradient Radon (G-Radon) with small amount of calculations and the high recognition rate as combination of the two methods. The conventional Radon transform is sensitive to translation and noise. Therefore we need to extract more robust feature such as gradient magnitude feature.

Section 2 presents the proposed gradient feature and Radon transform. Conventional Radon and G-Radon is compared for the rotated infrared targets images. After performing the G-radon, we compare features of upright targets and those of rotated targets. Section 3 validates the effectiveness of G-Radon for the synthetic infrared data set by comparing with the results using traditional Radon transform. Only an upright target image per target was used for the model learning and rotated 72 different target images were used for testing. The proposed G-radon transform, conventional Radon transform and Zernike moments are compared using confusion matrices. Through the experiments, we can validate the superior performance of the proposed G-radon feature. Section 4 concludes this paper and discusses about future works. The ultimate goal of this research is to achieve an improved ground target recognition and classification through the fusion of SAR/IR sensor information. This paper validates the target recognition for IR dataset only. In the future, we will verify the effects of SAR/IR fusion in ATR.

2 Proposed G-radon based ATR

The proposed feature extraction method is called G-radon. We use image gradients to extract targets' edge information for effective target recognition and compute gradient magnitude values. Next we perform the Radon transform and extract rotation invariant feature.

2.1 Gradient feature extraction

The directional gradients, G_x and G_y, are extracted from an image to obtain edge information. Edge magnitude is calculated eq. (1).

$$f(x,y) = \sqrt{(G_x^2(x,y) + G_y^2(x,y))} \qquad (1)$$

Fig. 1 shows the edge extraction results for a test image (Fig. 1(a)). Fig. 1(b) presents the gradient image in the x-axis direction. The value on the left side of the image is positive value because the intensity of background is lower value and that of the target is higher value. Fig. 1(c) shows the gradient result in the y-axis direction. Fig. 1(d) represents the computed edge magnitude value using eq. (1).

(a)   (b)

(c)   (d)

Figure 1. (a) Original input image, (b) computed row directional gradient result, (c) computed column directional gradient result, (d) gradient magnitude.
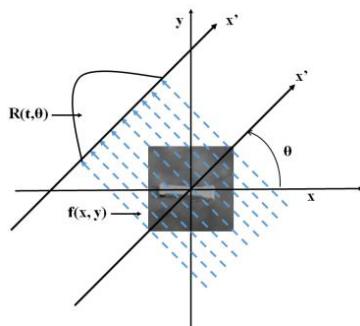
2.2 Rotation invariant Radon transform

Figure 2. Radon transform of a two-dimensional function *f(x,y)*.

Radon transform [17] accumulates image in Radon transform space as shown Fig. 2. The extraction process is simple and the feature is robust to image noise due to the integral property. The radon transform defined as

$$R(t,\theta) = \int_{-\infty}^{\infty}\int_{-\infty}^{\infty} f(x,y)\delta(t - x\cos - y\sin\theta)dxdy \quad (2)$$

where t is the perpendicular distance for a straight line from the origin, θ is the angle between the distance vector and the x-axis. Range of θ is 0 to π. *R(ρ,θ)* is the projection data obtained by the image curvilinear integral.

δ means dirac delta function. In each θ, gradient image *f(x,y)* can be expressed as follows
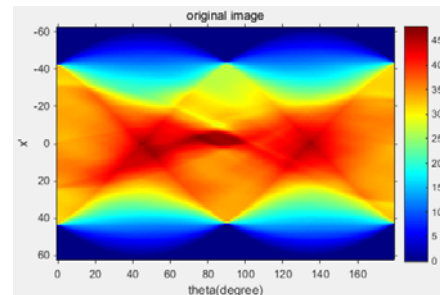
$$R(\rho,\theta) = \int_{-\infty}^{\infty}\int_{-\infty}^{\infty} f(\rho\cos - \rho\sin\theta, \ \rho\sin\theta + u\sin\theta)\delta(0)dxdy \qquad (3)$$

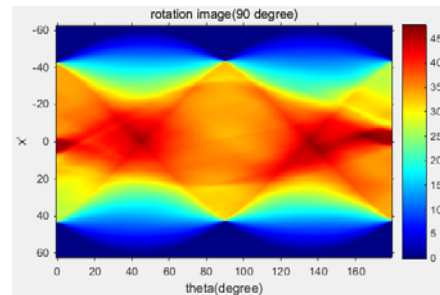when *x=1*, the delta function is 0. So it is converted to the following equation

$$R(\rho,\theta) = \int_{-\infty}^{\infty}\int_{-\infty}^{\infty} f(\rho\cos\theta - u\sin\theta, \rho\sin\theta + u\sin\theta)dud\rho \qquad (4)$$

when the image is rotated by θ_0 , Radon transform's projection data is also rotated by θ_0.

$$R(\rho,\theta + \theta_0) \qquad (5)$$

(a)

(b)

Figure 3. (a) Non-rotated image(0°), (b)Rotated image (90°).

Therefore radon transform is rotation invariant. Fig. 3 shows the application of Radon transform. Fig. 3(a) is a non-rotated image (0∘). High value is distributed from 30° to 150°. These values are the values accumulated in radon space. The value is distributed differently according to the shape of target. Fig. 3(b) is a rotated image (90∘). High value is distributed from 120° to 180° and from 0° to 60. Radon space is moved as much as the image is rotated.

The Fig. 4 shows the results of G-radon for the Bus (one is upright position, the other is rotated by 30°) and a fire truck (upright position). Blue solid line indicates the result of the Bus (0), orange broken line represents the result of the Bus (30) and yellow line with a circular mark indicates the fire truck (0). Bus (0) denotes upright position and Bus (30) represents an image rotated by 30°. The blue solid line show almost the same feature profiles as the orange broken line, but the yellow line with a circular mark show a different feature profiles. We can see that the result of G-radon is dependent on shape of target regardless of angle.
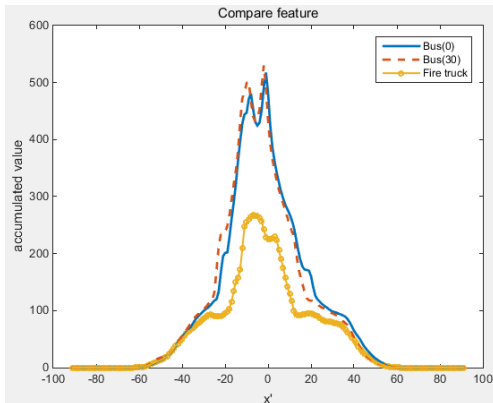
Figure 4. Comparison results of G-Radon for different targets with different rotations.

3 Experimental results

This section presents experimental results tested on synthesized IR image dataset. We show results of G-radon according to the number of targets. Finally, we show improved results by comparing G-radon with traditional methods such as Radon transform and Zernike moments.

3.1 Infrared target dataset

Infrared target dataset was prepared using a synthesis tool, OKTAL-SE [18, 19]. OKTAL-SE can synthesize a desired image using user's desired parameters such as season, weather, time, temperature, atmosphere environment, and thermal noise. Fig. 5 shows the processing flow of the scenario generator using OKTAL-SE. First, we insert 3D information such as building, terrain information and environmental information such as atmospheric radiation, temperature and special effects information such as cloud, fog, and image noise on the scenario generator. We create a Radiative Atmospheric file with the input parameter by using the SE-ATMOSPHERE. The resulting file is a scenario environmental information. It is used to create the scenario in the SE-SCENARIO. If you enter the desired targets and trajectories to build a test environment, it can provide an image of the simulated environment. Then, we create a synthetic image with a desire spectral band and sensor information using SE-RAY-IR. The resulting synthesized image can be found and added to the sensor noise in SE-SIGNAL-VIEWER.
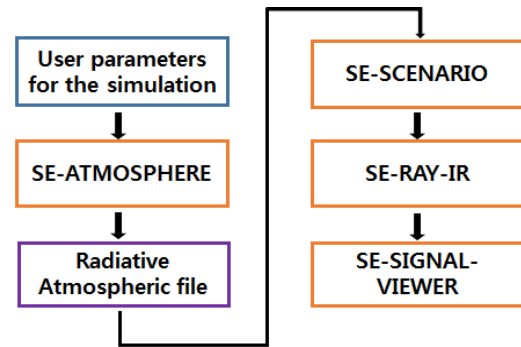
Figure 5. The synthetic infrared image generation flow using OKTAL-SE.

Target images are synthesized in the MWIR spectral band. Synthesis environment was created for the summer, fine, 10am. Other atmospheric environment, trajectory and special effect were not added. The pose of the IR camera was set at view point 0°, altitude 4km. Figure 6 shows the results of synthesized images. Dataset consists of 20 types of military targets and normal vehicles. The dimension of target data is 30 by 30 pixels. Each target is rotated by 72 different orientation in azimuth (0°, 5°, …, 350°, 355°) from a fixed range. In the experiments, we separate dataset into train data (upright image) and test data (rotated images). Train data is learned and randomly pick out a target in test data.
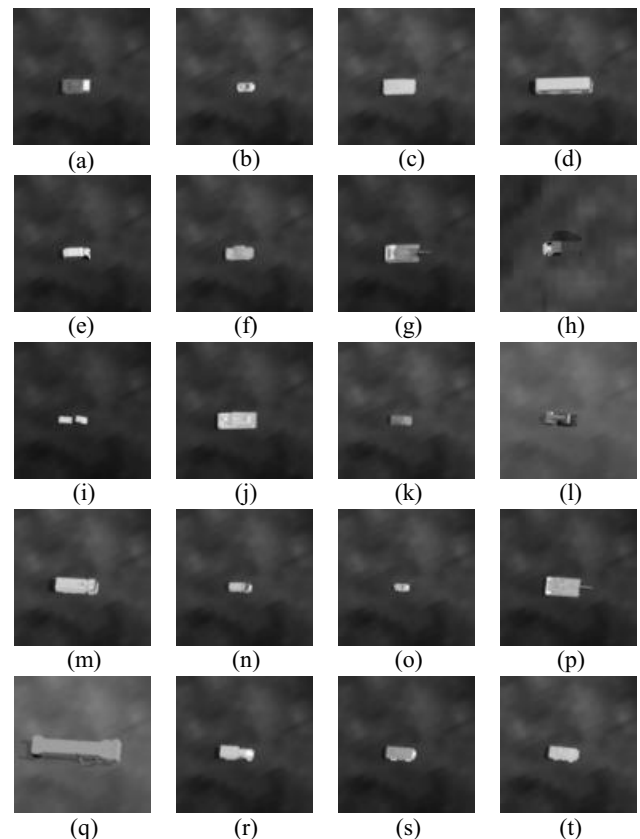
Figure 6. IR target Data set in MWIR: (a) 2s6-tunguska-sa-19lnch_camo, (b) 9s80m-dogear-radar_ca mo, (c) a10-thunderbolt-fighter_usaf, (d) ah64d-apache- attk_army-od, (e) AMX_10, (f) audi_tt, (g) backstairs_ car, (h) bag_car02, (i) BMP_3, (j) bus, (k) expert, (l) fire_ truck1, (m) firetruck, (n) ford_transit, (o) jeep, (p) leclerc, (q) naut_gangway, (r) su25, (s) T_72, (t) TMM.

3.2 Recognition performance

We compare the recognition rate of the traditional radon in order to confirm the performance of the proposed method for the different number of targets. We use a k-nearest neighbour classifier (k-NN, k=1) as a simple classifier. As shown in Fig. 7, the conventional Radon transform shows lower recognition rate than the proposed G-radon according to the number of test targets. The conventional Radon showed the recognition rate, 46%, for the 20 kinds of targets. The proposed method's recognition rate is also decreased depending on the number of targets. However, the proposed method's performance is better than the traditional method. The G-Radon showed the recognition rate, 68.2%, for the 20 kinds of targets. This result is 20% higher than the traditional method. The recognition rate curve of the G-radon decreases slowly than that of the Radon transform. The recognition result of each method on the number of target from 20 to 12 is shown in Table I.
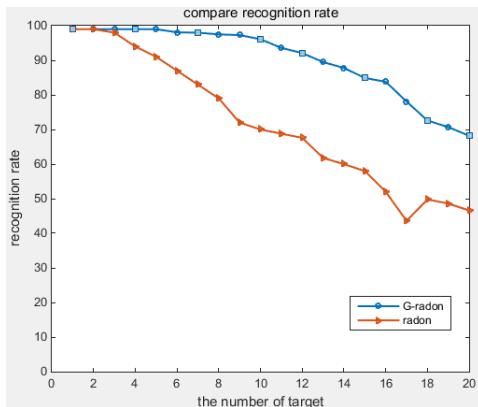

Figure 7. Recognition rate for G-radon and Radon transform.

Table 1. Comparisons of recognition rate

# of target	Proposed G-radon	Radon transform	Zernike transform
20	68.2	46.6	36.3
18	72.6	49.8	38
16	83.8	52	41.2
14	87.8	60	48.2
12	92.1	67.6	50.9

Fig. 8 show the recognition rate when the target is 10 as a confusion matrix for G-radon. The number of y-axis represents the true IDs of test targets and that of x-axis represents presented (recognized) IDs. The red color represents 100% of recognition rate and the blue color represents 0% of recognition rate. In figure 8, predicted values of the G-radon represents the red color. This result means that the predicted IDs are almost same true IDs. In Fig. 9 show the recognition rate for Radon transform. Only a few of the predicted values show a high recognition rate of 80% or more. Other predicted values represent recognition rate of 50% or less. In Fig. 10, the predicted values of Zernike transform are scattered. Most of the targets are not recognized.
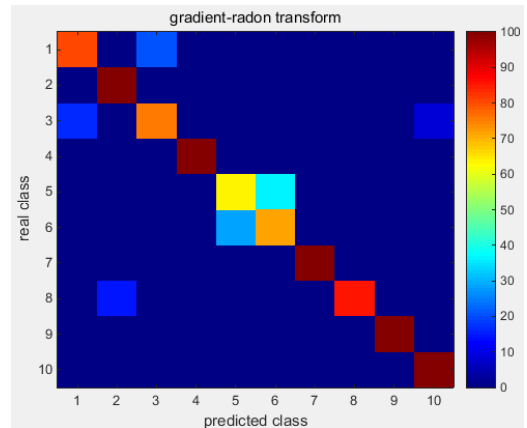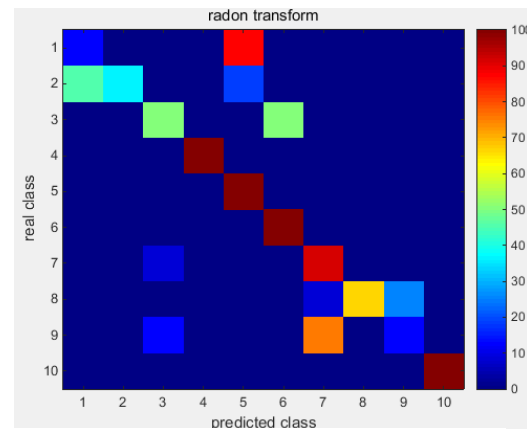

Figure 8. Confusion matrix of the proposed G-Radon.

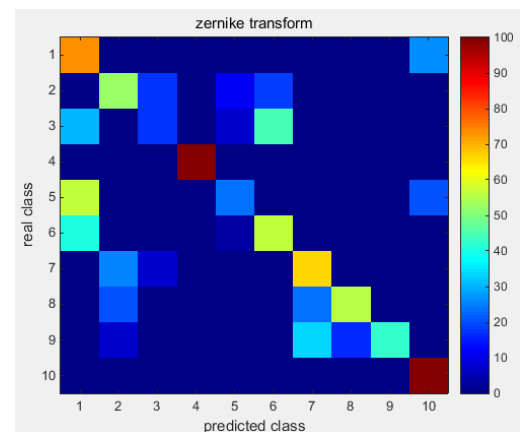**Figure 9.** Confusion matrix of Radon transform

Figure 10. Confusion matrix of Zernike moments.

4 Conclusions and future works

This paper proposes a new rotation invariant algorithm, G-radon, to achieve effective recognition. G-radon extracts gradient magnitude value and then computes Radon transform. We compare the recognition rate of the traditional Radon for the different number of targets to confirm the performance of the proposed method. According to the recognition test on the synthesized infrared dataset, the proposed G-Radon shows upgrade rotation invariance compared with the conventional Radon transform and Zernike moments. In future, we will combine the advantages of HOG and rotation invariant descriptor and consider the development of robust

algorithms for noise. The ultimate goal of the research is to achieve the improved ground target recognition and classification through the fusion of SAR/IR sensor information. This paper validate the target recognition for IR dataset only. In the future, we will verify the effectiveness SAR/IR sensor fusion for ATR problem.

Acknowledgement

References

1. F. Zhang, S. Liu, D. Wang, W. Guan, Image and Vision Computing, **27**, 4 (2009).

2. M. N. A. Khan, G. Fan, D. R. Heisterkamp, L. Yu, Computer Vision and Pattern Recognition Workshops (CVPRW), (2014).

3. P. Bharadwaj, L. Carin, IEEE Transactions on,Pattern Analysis and Machine Intelligence, **24**, 10 (2002)

4. Y. Lamdan, H. J. Wolfson, 2nd International Conference on Computer Vision (1988).

5. L. A. Chan, N. M. Nasrabadi,. International Journal on Artificial Intelligence Tools, **6**, 2 (1997).

6. Q. Zhao, J. C. Principe, IEEE Transactions on Aerospace and Electronic Systems, **37**, 2 (2001).

7. N. Dalal, B. Triggs, IEEE Computer Society Conference on Computer Vision and Pattern Recognition, (2005).

8. X. Wang, B. Xiao, J. F. Ma, X. L. Bi, Pattern Recognition, **40**, 12 (2007).

9. M. K. Hu, IRE Transactions on Information Theory, 8, 2 (1962).

10. J. Flusser, Pattern recognition, **33**, 9 (2000).

11. J. Flusser, Pattern Recognition, **35,** 12 (2002).

12. C. Kan, M. D. Srinath, Pattern recognition, **35**,1 (2002).

13. C. H. Teh, R. T. Chin, IEEE Transactions on Pattern Analysis and Machine Intelligence,**10**, 4 (1988).

14. R. Mukundan, S. H. Ong, P. A. Lee, IEEE Transactions on Image Processing, **10**, 9 (2001).

15. S. H. Weon, G. Y. Kim, H. I. Choi, Digital Contents Society, **12**, 3 (2011).

16. D. G. Lowe, International journal of computer vision, **60**, 2 (2004).

17. HØILUND, Carsten. The radon transform. Aalborg University, Vision, Graphics and Interactive Systems (VGIS), November, 12, (2007).

18. J. Latger, T. Cathala, N. Douchin, A. L. Goff, Defense and Security Symposium (pp. 654302-654302). International Society for Optics and Photonics, (2007).

19. J. J. Won, S. Kim, Synthetic SAR/IR Database Generation for sensor fusion-based A.T.R. (2014).